Intracoronary Optical Diagnostics

JACC: CARDIOVASCULAR INTERVENTIONS
VOL. 4, NO. 12, 2011

ISSN 1936-8798/$36.00
PUBLISHED BY ELSEVIER INC.
DOI: 10.1016/j.jcin.2011.08.015

STATE-OF-THE-ART PAPER

Intracoronary Optical Diagnostics

Current Status, Limitations, and Potential

Harry C. Lowe, MBChB, PhD,* Jagat Narula, MD, PhD,† James G. Fujimoto, PhD,‡ Ik-Kyung Jang, MD, PhD§

Sydney, New South Wales, Australia; Irvine, California; and Boston, Massachusetts

Optical coherence tomography (OCT), is a novel intravascular imaging modality analogous to intravascular ultrasound but uses light instead of sound. This review details the background, development, and status of current investigation using OCT, and discusses advantages, limitations, and likely future developments. It provides indications for possible future clinical use, and places OCT in the context of current intravascular imaging in what is a rapidly changing field of investigation. (J Am Coll Cardiol Intv 2011;4:1257–70) © 2011 by the American College of Cardiology Foundation

Optical coherence tomography (OCT), like intravascular ultrasound (IVUS) nearly 2 decades ago, is changing the way we see coronary pathophysiology. The detail with which coronary pathophysiology is viewed by this intravascular imaging modality is unprecedented, such that we are only now just beginning to establish how this imaging information might be best used to guide management and influence patient outcomes. This review, therefore, describes the current status of coronary optical diagnosis with OCT, in what is already a rapidly evolving and dynamic field of intracoronary imaging.

OCT Technology

OCT is an imaging technology analogous to IVUS but uses light instead of sound. It was first described by Huang et al. (1) in 1991, with its first application as single-plane cross-sectional imaging of the retina. OCT has since become an established imaging modality in clinical ophthalmology (2), and its biomedical applications have broadened to include gastrointestinal, dermatological, and intravascular imaging (3–5). Intravascular imaging has progressed to the stage where commercially available systems are now approved for use in Europe, Asia, and Australasia, and was recently approved in the United States.

The light source used for OCT imaging is in the near-infrared range, around 1,300-nm wavelength, selected as a compromise to achieve both penetration and delineation of vascular structures. Images are formed by measuring the magnitude and echo time delay of a reflected backscattered light signal in a manner analogous to IVUS. However, since the speed of light (3×10^8 m/s) is several orders of magnitude faster than that of sound (1.5×10^3 m/s), an interferometer is required to record the reflected light echoes (4). The interferometer splits the emitted light source into a reference and sample beam; the reference beam is directed to a reference mirror at known distance, the sample beam is directed to the structures of interest. The sample beam is then reflected back to a detector where it is summed with the reference beam, producing interference (4,6) (Fig. 1A).

Early commercially available versions of the technology used time domain (TD) detection. TD OCT employs a broadband light source with wavelengths centered around 1,300 nm, and a

From the *Concord Repatriation General Hospital and University of Sydney, Sydney, New South Wales, Australia; †University of California, Irvine School of Medicine, Irvine, California; ‡Massachusetts Institute of Technology, Cambridge, Massachusetts; and the §Massachusetts General Hospital and Harvard Medical School, Boston, Massachusetts. Dr. Jang has received research grants from LightLab Imaging, Abbott Vascular, and Johnson & Johnson; and he has received royalties from IP owned by MIT and licenced to LightLab Imaging/St. Jude Medical. All other authors have reported that they have no relationships relevant to the contents of this paper to disclose.

Manuscript received March 11, 2011; revised manuscript received August 4, 2011, accepted August 18, 2011.

reference mirror that is scanned to sequentially measure echoes from different depths (6,7). Currently available systems use a much higher speed method, known as frequency or Fourier domain (FD) detection. FD OCT uses an interferometer with a stationary reference mirror, but the light source frequency or wavelength is rapidly swept in time across 1,250 to 1,350 nm, such that received, reflected signals echo signals from different depths produced by different frequencies from the interferometer. Spatial features are encoded in frequency, in a manner somewhat analogous to magnetic resonance imaging. Axial depth profiles are then reconstructed by Fourier transformation. FD OCT thus essentially measures all echoes of light from different depths simultaneously, rather than sequentially as in TD OCT (Fig. 1B). FD OCT, therefore, achieves a dramatic improvement in sensitivity, enabling imaging speeds that are >10 times faster than TD OCT (6,8). This has been a key advance in clinical applicability, meaning that image acquisition is now possible during a contrast or saline flush lasting 3 to 5 s.

Abbreviations and Acronyms

ACS = acute coronary syndrome(s)
BMS = bare-metal stent(s)
DES = drug-eluting stent(s)
FD = Fourier domain
IVUS = intravascular ultrasound
NI = neointima
NSTEMI = non–ST-segment elevation myocardial infarction
OCT = optical coherence tomography
PCI = percutaneous coronary intervention
SAP = stable angina pectoris
STEMI = ST-segment elevation myocardial infarction
TCFA = thin-cap fibroatheroma
TD = time domain

OCT Image Acquisition

Since blood strongly scatters light, intravascular OCT requires a blood-free field lasting several seconds to allow imaging. In the earlier TD OCT systems, this was achieved either by injecting continuous saline/contrast flushes through the guiding or delivery catheters, or by using a proximal balloon occlusion of the vessel with distal saline/contrast injection. These techniques are safe, including in patients with acute coronary syndromes (ACS), but may be time-consuming, and require a high degree of operator expertise (9,10).

Conversely, FD OCT systems do not require proximal occlusion. The coronary vessel is transiently rendered free of blood by a bolus injection of saline, contrast, or other solution, injected at rates of 2 to 4 ml/s, and an automated 20 mm/s pullback within a monorail rapid exchange catheter allows imaging of a 6-cm-long coronary segment during a 3-s injection (8). The monorail rapid exchange catheter is compatible with 6-F guiding catheters, and can be conveniently incorporated into most interventional procedures. A summary of the characteristics of the FD OCT and TD OCT systems are shown in Table 1 (11). FD systems are being developed by various manufacturers (Lightlab, West-

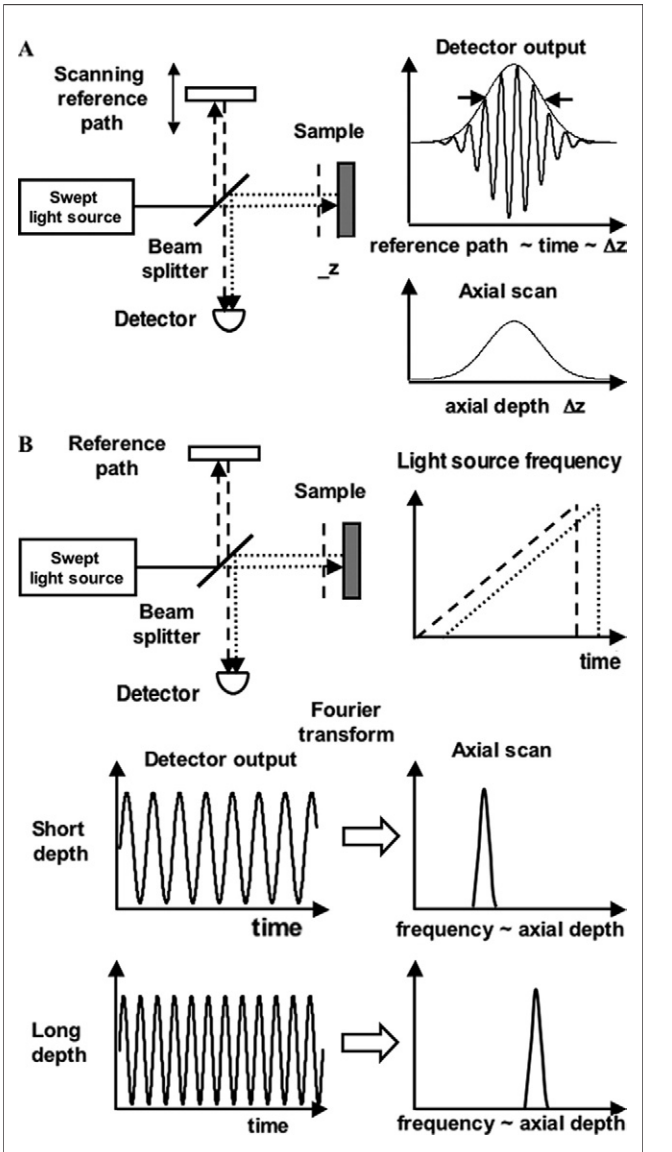

Figure 1. TD OCT and FD OCT: Schematic

(A) Time domain (TD) optical coherence tomography (OCT). Time domain OCT measures light echoes using a scanning interferometer. A low-coherence, broadband light source is split into 2 beams, 1 directed onto the tissue and the other onto a reference mirror. Interference occurs between backscattered light from the tissue and light traveling a known echo time delay from the reference mirror. Interference occurs only when the light from the sample arrives at the same time as light from the reference path. The magnitude and echo time delay of light from the tissue is measured by scanning the reference path, generating an axial scan. In an actual OCT instrument, the interferometer is built using optical fibers, and imaging is performed using an intravascular catheter with a rotating optical fiber and microlens in a transparent sheath. **(B)** Fourier domain (FD) OCT. Frequency or FD detection uses a frequency swept light source. The light is directed onto the tissue and a reference mirror at a fixed delay. Light echoes from different tissue depths return with different delays, resulting in a frequency difference between the signal and reference light. The interference produces a beat frequency (equal to this frequency difference) that depends on the echo delay. The beat frequency is measured by Fourier transforming the signal to recover the echo delay. Each sweep of the laser, therefore, generates an axial scan. Since all echoes are measured simultaneously, the sensitivity is dramatically increased.

Table 1. Comparison of IVUS and OCT

	IVUS	TD OCT	FD OCT
Energy wave	Ultrasound	Near-infrared	Near-infrared
Wavelength, μm	35–80	1.3	1.3
Resolution, axial/lateral, μm	100/200	15/90	15/20–40
Frame rate, frames/s	30	16–20	100
Pullback rate, mm/s	0.5–1.0	1–3	20
Axial scans, ×1,000		3.2–4.8	5.4
Lines, axial scans/frame		200–40	500
Maximum scan diameter, mm	10	6.8	9.7
Tissue penetration, mm	10	1–2.5	2.0–3.5

Axial resolution is measured in tissue. Scan diameter is measured in saline for time domain (TD) optical coherence tomography (OCT) and in contrast medium for Fourier domain (FD) OCT. Sources: Schuman et al. (2), Morgensen et al. (5), and Jang (11), and Lightlab, Westford, MA.
IVUS = intravascular ultrasound.

ford, Massachusetts; Terumo, Tokyo, Japan; and Volcano, Rancho Cordova, California) (12).

Ex Vivo Plaque Characterization

Characterization of plaque type. Fundamental to in vivo use of OCT is the validation of the technique using histological controls. The earliest study comparing OCT images of plaque with histology and suggesting applications for intravascular imaging was performed in 1996 (7). Comprehensive ex vivo comparisons date from 2002 and are outlined with comparisons to IVUS in Table 2. In an initial study, 357 atherosclerotic segments were derived from 90 cadavers, comprising 162 aortae, 105 carotid, and 90 coronary vessels (13). Three plaque types were identified, as fibrous, fibrocalcific, and lipid rich (Fig. 2). An initial training set of 50 specimens was used, then the 307 test specimens were examined blindly. Identification of fibrocalcific (96%, 97%) and lipid-rich (90%, 92%) plaques achieved high sensitivity and specificity, respectively, and although sensitivity for fibrous plaque was slightly lower (79%), specificity remained high (97%); interobserver and intraobserver agreements were acceptable (K = 0.88 and K = 0.91, respectively) (13). Although some subsequent studies have demonstrated similar diagnostic accuracy of OCT examination (14,15), others have found lower sensitivities, particularly in the differentiation of lipid from calcific plaque components (16,17) (Table 2). The lower sensitivity may result in part because of small sample size or methologic differences (18,19). The differentiation of lipid and calcific plaque may require expertise because both are characterized by signal attenuation, wherein the lipid areas have relatively diffuse borders, and calcific plaques have sharper edge definition (13,16). Most studies have been performed using the initial imaging systems: validation using FD OCT systems is ongoing, with the diagnostic accuracy likely to be superior with improved imaging technology.

Characterization of fibrous cap thickness. Given the association of cap thickness of <65 μm adjacent to the site of plaque rupture in 95% of cases (20), there is interest in the ability of OCT to accurately detect fibrous cap thickness (4,12,21,22). Two studies totaling 64 lipid-rich plaques have demonstrated close correlation between OCT imaging and histology in the assessment of cap thickness ($r = 0.89$ and $r = 0.90$, $p < 0.001$) (4,21). This represents a unique ability of OCT for the assessment of high-risk plaques.

Table 2. Ex Vivo Plaque Characterization With OCT and IVUS Compared With Histology

	Plaque Types			
First Author (Ref. #)	Lipid	Fibrous	Calcific	Comments
Yabushita et al. (13)				
OCT	90/92	96/97	79/97	357 segments from 90 cadavers; included coronary, aorta, carotid; training set of 50
Kume et al. (14)				
OCT	85/94	96/88	79/99	166 coronary segments, no training set
IVUS	59/97	88/86	98/96	
Kawasaki et al. (15)				
OCT	95/98	98/94	100/100	128 segments from 17 cadavers; no training set; same readers as the Yabushita group
IVUS	67/95	93/61	100/99	
IB IVUS	84/97	94/84	100/99	
Rieber et al. (17)				
OCT	77/94	67/97	64/88	17 segments from 8 in situ arteries, multiple images
IVUS	10*/96	63/59*	76/98	
Manfrini et al. (16)				
OCT	45/83†	83/82	68/76	79 coronary segments from 15 cadavers; 11-segment training set

Numbers indicate percent sensitivity/specificity for detection of each plaque type. *Significant difference in comparison between OCT and IVUS ($p < 0.05$). †American Heart Association classification type IV and Va, indicating lipid plaque. Adapted, with permission, from Chen et al. (3).
IB = integrated backscatter; other abbreviations as in Table 1.

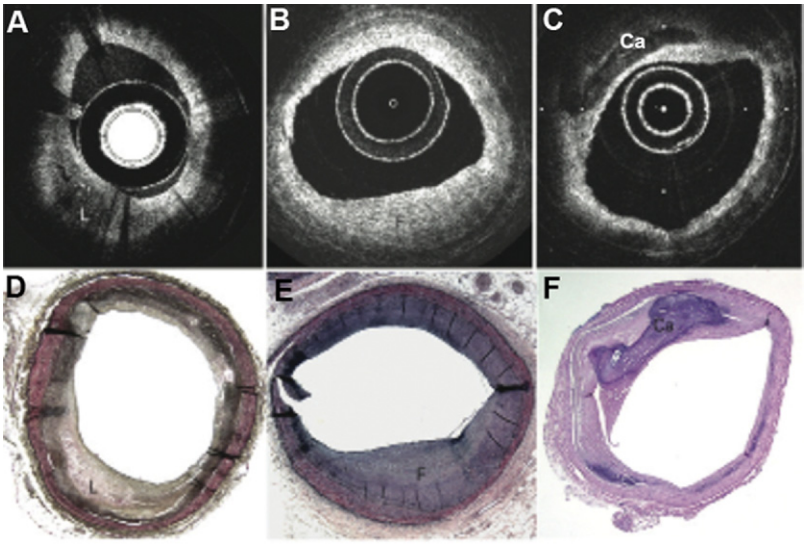

Figure 2. Plaque Characterization

Optical coherence tomography images for lipid-rich **(A)**, fibrous **(B)**, and calcific **(C)** plaque types with corresponding histological sections **(D to F)**. Calcium-containing (Ca) regions appear as signal-poor regions within the vessel wall. Lipid-rich plaque has diffuse borders, whereas calcific regions have sharply demarcated edges. Histological sections: **(D and E)** Movat pentachrome, **(F)** hematoxylin and eosin. Original magnification × 2. Adapted from references Raffel et al. (4) and Yabushita et al. (13).

Characterization of thrombus. In initial studies, intraluminal thrombus was compared to pathological specimens and confirmed as irregular, signal-rich regions (23,24). Using a measure of signal attenuation, a distinction is possible between white (platelet-rich) thrombus with low backscatter and red (platelet-poor) thrombus with higher backscatter in signal attenuation or shadowing deeper into the thrombus (22). In vivo, this distinction is less evident (12), with thrombus almost always of a mixed type. Of interest, small mural thrombi may often be seen.

Characterization of intralesional macrophages. Macrophage/foam cells, which are large (diameter: 20 to 30 μm) cells and contain multiple lipid-rich bodies, produce a high signal variance from the surrounding tissue to potentially allow a direct visualization of macrophages with OCT (18). The normalized standard deviation of the OCT signal within the fibrous cap was used to estimate macrophage concentration in lipid-rich plaques and compared with CD68-positive macrophage cell counts assessed immunohistochemically; there was a good correlation ($r = 0.80$, $p < 0.001$) (18). This is a finding of particular interest, though clearly it is important to recognize that at present, the resolution is not high enough to recognize individual macrophages, and such correlations are valid only for comparisons within plaque and not the vasculature in general, and may be dependent on the OCT system (12,19).

Limitations in image interpretation. Ex vivo histopathological correlative studies suggest 2 principal limitations in image interpretation. First, the differentiation of lipid from calcium deposits may be difficult. Calcium is typically identified with signal-poor areas, with sharply defined edges; lipid by similarly signal-poor areas, though with diffuse borders (13,16). On occasion, the characterization of borders may be difficult. Second, plaque visualization may be problematic when fibrous plaque is thick (16). As a result of poor tissue penetration, it can be difficult to distinguish deep lipid from attenuated bulky fibrous plaque. For the same reason, it is often impossible to accurately measure plaque burden and to study development of neovascularization from adventitia. Whether such limitations exist with current-generation imaging systems is under investigation at present.

In Vivo Plaque Characterization

Based on the ex vivo correlative information, there has been a great interest in the ability of OCT to allow atherosclerotic plaque characterization in vivo, even though it has limited depth penetration (1 to 2.5 mm) (Fig. 3). Following the initial proof-of-principle study of OCT in normal pig coronary vessels in vivo (25), the first human studies were performed in 2002 in patients with mild to moderate atherosclerotic lesions (22), which demonstrated the safety of OCT and efficacy in the identification of the normal vessel wall and plaque components in vivo (22). The normal vessel was well seen with OCT as a trilaminar structure of intima, media, and adventitia; the media was visible as a relatively low-signal middle layer (26). On this background, some of the early stages of atheromatous

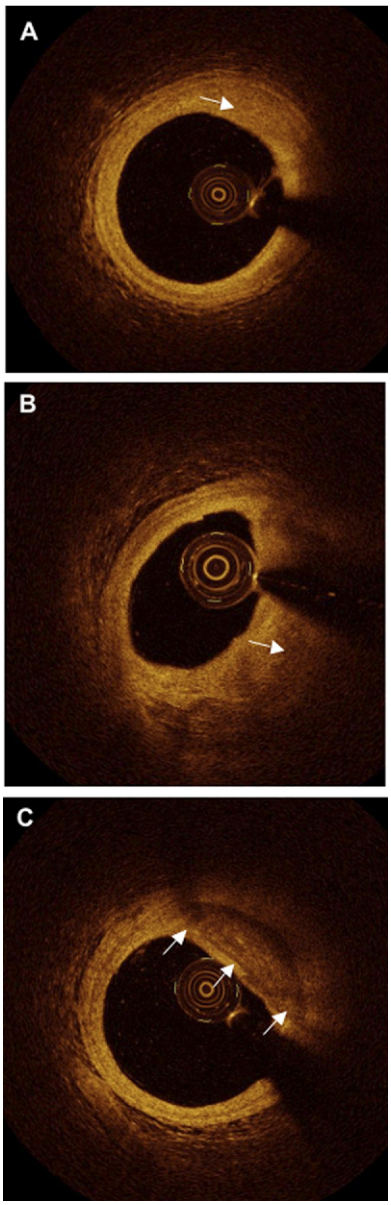

Figure 3. In Vivo Plaque Characterization

(A) Fibrous plaque. Homogeneous high-intensity signal **(arrow)**. **(B)** Lipid-laden plaque. Low-intensity, irregular signal with indistinct and irregular borders **(arrow)**. **(C)** Calcified plaque. Low-intensity, sharp bordered, "textured" appearances (marked by the **3 arrows**).

change, including intimal thickening are also well visualized; these observations form part of a recent consensus document (26).

Characterization of plaque type. Plaque type identified by OCT has been compared in various patient cohorts (27). Given the superficial penetration of OCT, lipid-rich plaque has been defined semiquantitatively only, as lipid comprising more than 2 quadrants (27). Using this definition, lipid-rich plaque was identified in 90% of ST-segment elevation myocardial infarction (STEMI) and 75% of non–ST-segment elevation myocardial infarction (NSTEMI), as compared with <60% of stable angina pectoris (SAP) lesions ($p = 0.09$) (27).

Characterization of fibrous cap thickness. Thin capped fibroatheromata (TCFA) are defined pathologically by the triad of a lipid core, a fibrous cap with a thickness <65 μm, and inflammatory cell infiltration of the fibrous cap (20). Interest has therefore focused on the use of OCT for in vivo assessment of fibrous cap thickness, given the limitations of IVUS, and OCT's unique ability to image superficial detail (4,12). In the ACS patients discussed in the previous text, TCFA was observed in 72% STEMI and 50% NSTEMI culprit lesions as compared with 20% SAP lesions ($p = 0.01$) (27). Presented another way, the same groups exhibited mean fibrous cap thicknesses of 47, 54, and 103 μm, respectively (27). Similar findings have been reported by subsequent studies (77% to 83% STEMI, 46% NSTEMI, and 3% to 25% SAP; $p = 0.001$) (10). These observations provide the first in vivo support for the key postmortem studies suggesting the association between ACS and TCFA, and provide 1 of the key advances that OCT has already provided as an intracoronary diagnostic tool.

These findings have also suggested the important potential for using OCT measurements of fibrous cap thickness as a possible marker of plaque vulnerability. In a single-center prospective study, cap thickness has been shown to increase in a statin-treated group (28), and in a smaller observational study, patients on statins had fewer plaque ruptures (8% vs. 36%) and had a trend toward increased fibrous cap thickness (78 μm vs. 49 μm) compared with those not taking statin (29). It is important to recognize that broad clinical outcome data are lacking to date, though it would appear possible that OCT will be incorporated in future plaque-stabilization and lipid-lowering therapy trials, with fibrous cap thickness being a potential surrogate endpoint.

Characterization of plaque rupture. The ability to detect plaque rupture with OCT has been suggested, and is a potentially important use of OCT. However, OCT-verified plaque rupture has been found with somewhat wide variation between types of ACS in different studies. Rupture has been observed in 25% to 73% for STEMI, 15% to 42% for NSTEMI, and 3% to 11% for SAP (10,27). Interestingly, in the OCT examination of culprit lesions in patients with ACS that occurs on exertion, OCT demonstrated rupture at the plaque shoulder in almost all patients, compared with one-half of the patients with ACS that occurs at rest ($p = 0.017$), suggesting the mechanisms of plaque rupture may be distinct between these patients (30). OCT has also demonstrated that in patients undergoing coronary stenting, OCT-verified TCFA was associated with periprocedural creatine kinase-MB rise, indicative of procedural plaque rupture or disruption and atheroembolization (31). The

potential for OCT to provide in vivo insights is evident from such observations, and likely means such lesional assessments by OCT will be an area of active investigation.

Identification of intralesional macrophages. Given the third component of the pathological definition of TCFA—that of inflammatory cell infiltration of the fibrous cap—there is interest in the ability of OCT to identify intralesional macrophages in vivo. Close correlation with macrophage density measured by CD68 stain versus OCT image was possible in selected lesions in vitro as discussed in Tearney et al. (18). in vivo, macrophage density is increased in ACS (both STEMI and NSTEMI) compared with SAP (32). These studies have not yet been replicated with the newer OCT devices, and depend on selection of a precise area of interrogation and offline analysis (33,34).

Image artifact. Artifactual images occur with OCT imaging. Easily remedied examples include inadequate blood flushing from the vessel, air in the imaging catheter sheath, and eccentric wire positioning producing a "merry go round" stent strut appearance. Examples of these and other image artifacts are illustrated in Figure 4. With increasing use of the novel OCT imaging systems, these and other limitations require clear identification to maintain image integrity.

Additional information from OCT imaging. There exists the potential for OCT to identify angiogenesis or neovascularization associated with atheroma. "Black holes" of between 50 and 300 μm, present in consecutive frames, appear to correlate histologically with small vessel formation (26,35), such that it is possible such information will be sought as part of OCT-based trials of lesion stabilization. Regarding OCT in the assessment of saphenous vein graft atheroma, though this is technically feasible, and has demonstrated utility in the small numbers studied to date (36,37), whether flushing under pressure during OCT imaging contributes to distal embolization remains to be established. If maximum scan diameters remain at 7 mm, this is also likely to limit widespread use of OCT in this context. Conversely, early work imaging arterial radial grafts suggests OCT appears safe, and has found the potentially important observation of acute injury and chronic thickening following radial-approach coronary intervention (38).

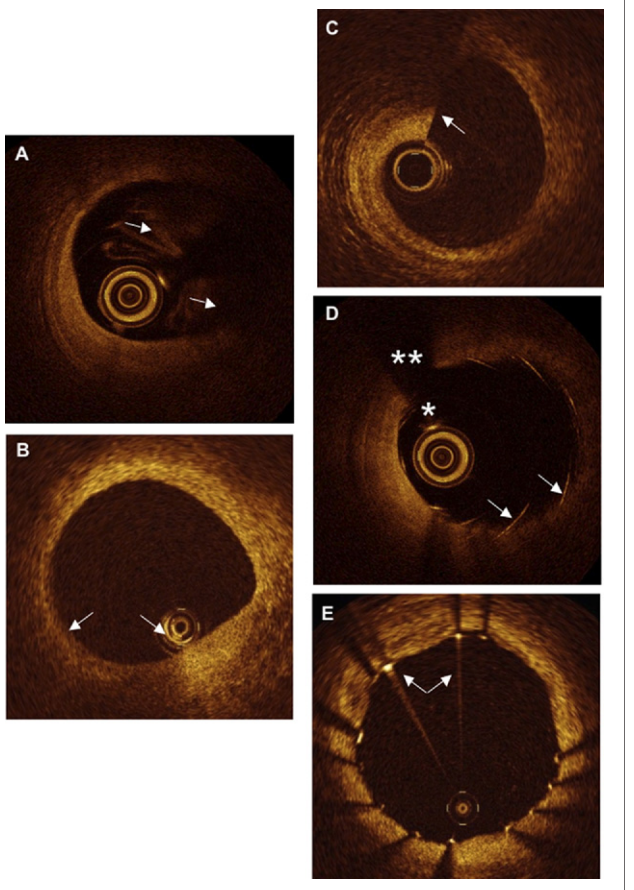

Figure 4. Image Artifact

(A) Blood contamination as a result of inadequate flushing **(arrows)**. There is a resultant distant image attenuation. **(B)** Bubble artifact as a result of air bubbles in the ImageWire sheath. This results in image attenuation **(arrow)**. **(C)** "Step-up" or "sew-up" artifact **(arrow)** as a result of relatively rapid vessel or wire movement during imaging. **(D)** Stent strut "merry go round" as a result of eccentric wire position, most marked with most distal struts **(arrows)**. **(E)** Saturation artifact, or blooming, as a result of highly reflectant structures, for example, stent struts **(arrows)**. Examples of wire position **(asterisk)** and wire shadow artifact **(double asterisks)** are shown in **D**.

OCT and Percutaneous Coronary Intervention: Immediate Post-Procedural Evaluation

Given the fine resolution at a superficial depth, OCT allows a uniquely detailed image of the effects of stent implantation on the vessel wall. OCT allows examination of the target vessel both pre- and post-intervention (39), defining stent struts readily, tissue prolapse between stent struts immediately (40), and tissue characterization of plaque before and after stent placement (41). The detail provided by the initial studies has led to wide interest in tissue prolapse, dissection; both intrastent and edge; thrombus; and stent strut malapposition (42). Many of these appear to occur frequently (42), and are illustrated in Figure 5.

Tissue prolapse. Tissue prolapse, or protrusion of tissue between stent struts without apparent surface disruption, is defined as occurring if the depth of protrusion is >50 μm, and has been observed almost universally (97.5%) at some point along the stented segment (42). This high frequency is similar to postmortem findings (94%) (43), but significantly higher than IVUS-verified prolapse of 18% to 35% (40,44), suggesting OCT is both sensitive and specific. The clinical significance of such prolapse is, however, unclear, given that it occurs so frequently, and has not been associated with early clinical events (42) nor examined in relation to late clinical events.

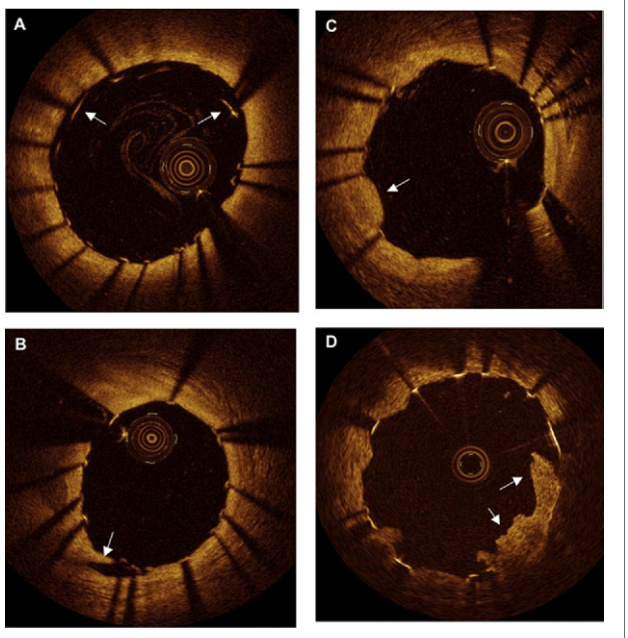

Figure 5. Immediate Post-Procedural Evaluation

(A) Malapposition. Stent strut malapposition **(arrows)** is clearly identified and can be quantified. Identifying small degrees of malapposition requires knowledge of stent strut thickness in that only the leading edge of a metallic stent strut is demonstrated with optical coherence tomography (OCT). **(B)** Stent edge dissection **(arrow)**. Detailed identification of dissection is seen with OCT. **(C)** Intrastrut prolapse **(arrow)**. Prolapse is defined as >50-μm projection of tissue from a line drawn between stent struts and is readily identified. **(D)** Thrombus **(arrow)**: irregular bordered, signal-intense regions identify thrombus.

Intrastent dissection. Intrastent dissection, defined as either disruption of the vessel surface with dissection flap, or association with an underlying cavity, has been observed at a similarly high frequency (87.5%), with 86.3% of stented vessels showing a dissection flap and 68.8% showing an underlying cavity at some point along their length (42). In-hospital clinical events were also absent in this group, meaning their significance—if any—remains to be established. Edge dissections were present less commonly (26.3%), with similarly no associated clinical events (42). For both tissue prolapse and dissection, there was no association with clinical presentation (42). Edge dissection is, however, variable, with plaque type as assessed by OCT being more frequent in fibrocalcific (43.8%) and lipid-rich (37.5%) compared with fibrous plaque (10%) (26,45).

Stent strut apposition/coverage. Given the precision with which OCT visualizes the leading edge of stent struts, and the lumen–vessel wall interface, the degree of stent strut apposition is being extensively evaluated using OCT by a number of investigators (4,8). A proposed 3-point classification defines stent strut apposition as embedded (when the leading edge is buried within the intima by more than one-half its thickness), protrusion (when the stent strut is apposed but not embedded), and malapposed (when there is no intimal contact) (46,47). Another classification, pertinent for follow-up studies examining the degree of neointima formation, describes whether or not the stent strut appears covered with tissue, and whether struts are well apposed or malapposed (48). Stent struts are, therefore, classified as: 1) well apposed and covered; 2) well apposed and not covered; 3) malapposed and not covered; and 4) malapposed but covered (Fig. 6) (12,48).

The degree of any malapposition has not been widely quantified, but with newer analysis software, this is easily performed, and measurement of the degree or distance of malapposition in microns is readily possible. Individual stent struts within sequential image frames are examined along the stent length, such that large datasets of strut-level analyses are generated. These examine stent strut position at hundreds of data points within an individual stent, with the potential for a more detailed analysis than perhaps even histology, given this provides information from 0.5- to 3-mm intervals between sections (49,50). Such measurements appear to have low intra- and interobserver variability, and with a number of software algorithms for quantitative analysis producing detailed stent strut apposition maps of potentially precise detail, there is the likelihood that 3-dimensional image reconstruction will be achievable, though clustering of data from individual stents within larger analyses requires careful statistical consideration (Fig. 7)

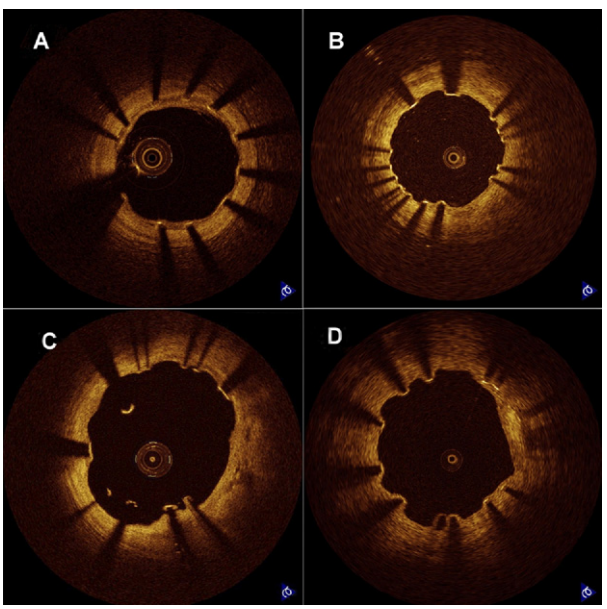

Figure 6. Stent Coverage

Enlarged images of individual stent struts illustrating classification of stent strut coverage. **(A)** Well apposed and covered; **(B)** well apposed and not covered; **(C)** malapposed and not covered; and **(D)** malapposed but covered.

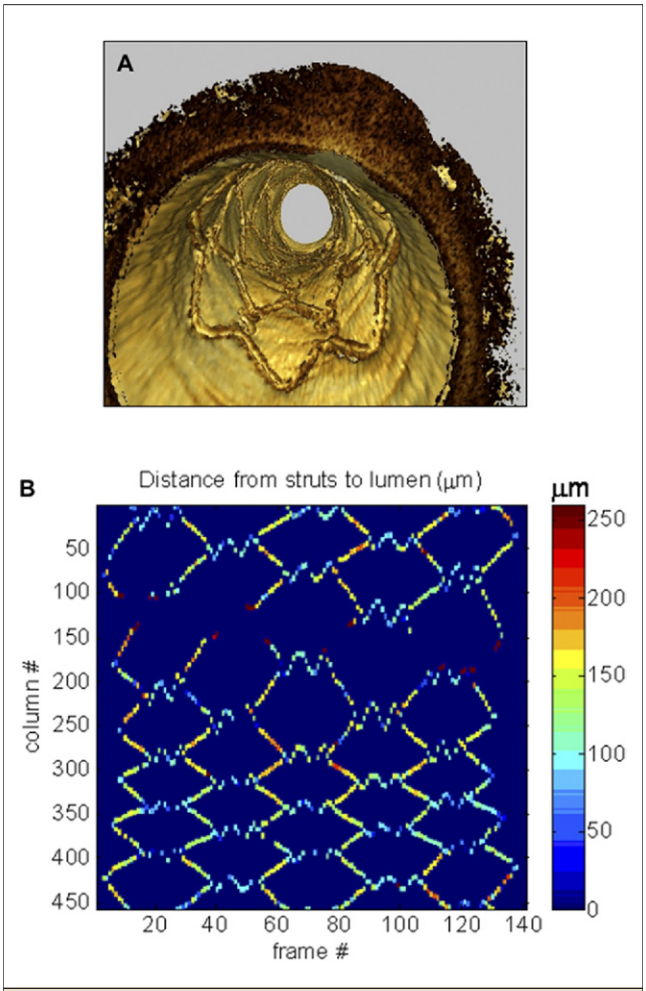

Figure 7. 3-D Stent Strut Analysis Reconstruction

(A) Example of current 3-dimensional (3-D) reconstruction technique. **(B)** Example of the results of the algorithm for individual stent strut analysis mapping, which color codes the distance of the stent strut from the vessel wall.

(8,51–53). In a small series of OCT examinations after drug-eluting stent (DES) implantation, in which more than 6,000 stent struts were examined, 57.1% struts were embedded, 33.8% were protruding, and 9.1% were malapposed (46). It is possible that both lesion or stent type plays a role in malapposition. The clinical relevance of these findings at present remains unclear.

OCT and PCI: Late Follow-Up

In-stent restenosis: quantification. Analysis of the long-term effects of stenting at the level of the stent strut is now possible with OCT, such that the amount of tissue coverage, degree of neointimal (NI) thickening, individual strut apposition, and associated findings are being defined in longitudinal studies and as endpoints in clinical trials (12,54). Some of these studies are summarized in Table 3. Though stent strut coverage does not necessarily equate with endothelialization, with this being below the resolution of OCT, nor even indicate at present the tissue type, these studies are aimed at optimizing stent performance, with modest, uniform, relatively nonprogressive stent coverage being the aim.

Stent strut coverage. Following initial work by Takano and others, stent strut coverage assessed by OCT has been performed in a number of studies. In studies comparing bare-metal stents (BMS) with DES, with follow-up of between 3 and 7 months, exposed struts with BMS are low (0.1% to 0.3%) (55,56). For DES, most data are available for sirolimus-eluting stents, and these have shown higher exposed strut rates of 4.9% to 17% (56–59), with 1 study suggesting reduced exposed strut rates with time after stent placement: 10.4% at 6 months, compared with 5.7% at 12 months (60). DES type may also influence stent coverage, with both paclitaxel- and zotarolimus-eluting stents exhibiting fewer exposed stent struts compared with sirolimus; 1 study has demonstrated a stent strut exposure rate of 0.3% at 9 months with zotarolimus compared with 12% for sirolimus (58,59). Zotarolimus-eluting stents may also have low rates of uncovered stent struts comparable to BMS in the setting of STEMI (54). Of importance, the ability of OCT to examine vascular responses, including stent coverage at sites of stent overlap, has been recently demonstrated, also suggesting differences between DES types (61,62). Intriguingly, in an animal study of OCT assessment of stent strut coverage, there was gradation of decreasing numbers of uncovered stents progressing distally along the stent, with 41.1%, 35.6%, and 24.3% of uncovered struts in the proximal, mid, and distal thirds of the stents, respectively (63).

It is important to be aware of the variable definition of strut coverage in various investigations. This is best exemplified in the same patient cohort in the LEADERS (Limus Eluted From A Durable versus ERodable Stent Coating) OCT substudy of a biolimus degradable polymer-coated stent; post-implantation lesions were defined as having any uncovered struts (63.3%), at least 5% uncovered struts

Table 3. Potential Clinical Utility for OCT

OCT recommended
Clinical trial evaluation post-stent
Clinical trial evaluation of novel plaque stabilizing agents
OCT could be considered
Characterization of coronary plaque
Evaluation of immediate post-PCI vascular status: dissection, stent strut expansion, stent strut apposition, thrombus
Assessment of late stent thrombosis risk: stent strut coverage, malapposition
Evaluation of other vasculatures: pulmonary, peripheral arterial, post-transplant vasculopathy
OCT may not be helpful
Assessment of left main stem stenosis severity
Assessment of saphenous vein graft atherosclerosis

OCT = optical coherence tomography; PCI = percutaneous coronary intervention.

(3.8%), or at least 10% uncovered struts (2.2%) (64). The former description may be too sensitive to have clinical relevance, but the latter may be more useful. Although histopathological correlations with stent strut coverage are at an early stage only, a number of important observations may already be made. OCT, like IVUS, may overestimate lumen area, and may vary with imaging technique (65) and possibly also with software analysis. Following stenting in normal pig coronary vessels using FD OCT, there appears a close correlation between OCT images and stent strut coverage assessed by both scanning electron microscopy and by histology (66). Although an early study with the TD OCT system suggested OCT imaging of shallow NI depths may underestimate stent coverage (63), this later work using FD OCT finds good agreement between OCT and histology in the assessment of NI thickness ($r = 0.90$, $p < 0.01$) and stent strut coverage ($r = 0.96$, $p < 0.01$) (66), so that these and other studies are providing precision in the measurement of NI thickness that is at the limit of axial resolution of OCT at 15 μm (59,66,67). Interestingly, in recent work, the density of the OCT image also provided useful information, with low-intensity signal that covers stent struts associated by scanning electron microscopy with fibrin, progressing to a higher-density signal, associated with NI formation by scanning electron microscopy, with increasing time post stent (66). Studies of this type show the potential for OCT to provide important insights into the pathobiological responses to stenting in vivo in the atheromatous human coronary.

Stent strut apposition. Malapposition was first defined as lack of contact between stent strut and intima, in a clinical setting, using IVUS criteria (68,69). To be used in OCT imaging, this requires recognition that only the leading edge of the stent strut is visible with OCT, such that precise definition of malapposition requires knowledge of stent geometry and thickness. This is pertinent, given that stent strut diameter varies, for example, Cypher (sirolimus; Cordis Corporation, Bridgewater, New Jersey) = 154 μm, Taxus (paclitaxel; Boston Scientific, Natick, Massachusetts) = 127 μm, Endeavor (zotarolimus; Medtronic, Minneapolis, Minnesota) = 107 μm, Xience (everolimus; Abbott Vascular, Santa Clara, California) = 88 μm. To date, there has been variation between study definitions (60,70), so that consensus in this area is currently being sought. However, such discussions again reflect the intravascular detail that OCT imaging is capable of providing.

The denominator of malapposed stent struts also varies between studies, variously being total stent struts or stented lesions (64,71). A common definition is the percentage of malapposed stent struts compared with total stent struts, and has been found to be between 0.2% and 2.6% for DES (59,71). Zotarolimus-eluting stents may have lower rates of malapposition compared with sirolimus (0.2% vs. 2.6% at 9 months) (59), and sirolimus may have a reducing rate of malapposition between 5 and 43 months (1.4% vs. 0.3%) (71).

Thrombus. Small areas consistent with intraluminal thrombus have been observed at follow-up after stenting using OCT. Given the limited ability of IVUS in this context, and recognition of ongoing risks of late stent thrombosis, these observations are of interest. Such thrombi are relatively small, and generally adjacent to the intima. Reported rates vary between 5.9% and 27.8% for sirolimus-eluting stents and 11% for paclitaxel-eluting stents (58,59,71–73); however, the sample size in all these studies has been very limited. Most of these studies have been within 1 year, with patients predominantly on dual antiplatelet therapy of aspirin and clopidogrel (58,59,72,73). The potential for OCT to detect the increased thrombotic risk later after DES is likely to be an area of ongoing interest.

Correlation with clinical outcomes. Of importance, how the OCT indexes of stent coverage, malapposition, thrombus, and NI formation correlate with clinical outcomes is not known. Interestingly, although zotarolimus-eluting stents have shown a higher rate of stent coverage compared with sirolimus-eluting stents at 9 months (59), this has not translated into improved clinical outcomes (74). Similarly, OCT-diagnosed intrastent thrombus—which might be expected to relate to minimal NI and uncovered stent struts—has shown no relationship to NI thickness (75). Such correlation of OCT findings with clinical outcomes is thus likely to be an area of ongoing investigation, with OCT substudy analyses of larger clinical trials already underway or reported. Such studies are likely to play an important role in advancing OCT from a research to a clinical tool.

In-stent restenosis: characterization. It has been suggested that OCT may provide characterization of in-stent restenosis tissue (76–78). In limited clinical studies to date, predominantly following DES, in-stent restenosis material has been described as uniformly homogeneous or heterogeneous; layered, with signal attenuation that may be gradual or rapid; or almost uniformly hypodense (76–79). Variation in appearance suggests variation in tissue composition. Pathological studies of human atherectomy specimens of in-stent restenosis tissue post-DES have shown a variety of tissue types, including smooth muscle cells, proteoglycan-rich myxomatous material, thrombus, and fibrinoid material (80). Substantial pathological correlates with OCT findings are not available, though in anecdotal reports, OCT regions of hypodense signal are related to myxomatous tissue, and hyperdense regions related to smooth muscle cell–rich NI (81); in a porcine study, hypodense OCT signal was associated with fibrinoid and proteoglycan material located in the peristent strut region (82). This capability of OCT to provide insight into histopathological changes following stenting, though preliminary, is of potentially great interest.

De novo atherosclerosis post-stenting. Of particular interest are recent observations of long-term follow-up (>5 years)

following bare metal stenting. In patients with OCT performed >5 years post-stent compared with patients with <6 months post-stent, OCT appearances suggest important differences (83). The late group had relatively high rates of lipid-laden intima, intimal disruption, and thrombus formation (67% vs. 0%, 38% vs. 0%, and 52% vs. 5%, respectively). Presumed intraluminal neovascularization was also more commonly seen in the late group (62% vs. 0%) and more commonly associated with lipid-laden intima than nonlipid-associated tissue (79% vs. 29%) (83). In separate studies, similar lipid-rich plaque has been observed in one-third of stents (16 of 39 patients) at 6.5 ± 1.3 years following BMS in patients presenting with recurrent ischemia (84). Interestingly, in these patients, the fibrous cap was also relatively thin (57.7 ± 5.8 μm) and widespread (lipid arc: 173° ± 58°), and a smaller number of patients had evidence of recent plaque rupture or mural thrombus (84). Interestingly, angioscopy and histopathological studies provide supportive evidence for similar observations after DES (85,86); in-stent de novo atherosclerosis was much more aggressive and occurred earlier with DES. Angioscopy has demonstrated increased yellow (i.e., lipid-containing) plaques in late (>4 years) follow-up after BMS compared with increased white (i.e., fibrous) plaque at early (<6 month) follow-up (85). Histopathological studies have demonstrated lipid-laden macrophage accumulation within NI formation after BMS and DES, with that in DES peaking at 1 year, and that following BMS only seen after 4 to 5 years (86). It is, therefore, conceivable that late OCT examination post-stent will provide useful pathobiological insight.

Study Limitations

A number of important limitations remain with OCT. A principal limitation is the need to displace blood or dilute the hematocrit, either with saline or contrast flush injection, or a combination of the two. Motorized imaging pullback has been a significant advance with FD systems, enabling efficient imaging during injection and is likely to see further improvement. However, the limitation of requiring a blood-free field is likely to remain in the near future, given that blood strongly scatters light. A second principal limitation to OCT is the shallow image penetration of 1 to 2.5 mm (26). This prevents assessments of cross-sectional plaque area, which may mean that OCT has only a limited role in the assessment of left main stem and saphenous vein graft atherosclerosis severity (87). Imaging the peripheral arterial bed has also not been reliable, particularly with the earlier generation systems. In addition, some aspects of plaque characterization still present difficulties with OCT. The differentiation of calcific areas from lipid pools can be problematic (16,26). Both result in a low attenuation signal, though lipid often has a more irregular border, but in direct comparisons with postmortem human samples, image interpretation may be difficult (16). Last, image artifacts do occur, including incomplete blood displacement; "sew-up" malalignment of the vessel as a result of excessive vessel or wire movement relative to imaging speed; image attenuation as a result of air; and others, well described previously (12).

The Potential for Clinical Utility

OCT is at present an investigative tool for intravascular imaging, providing unique detail of relatively superficial intravascular structure. At a practical level, it is easily incorporated into interventional procedures, with minimal additional training, and has recently gained widespread regulatory approval. Although these features mean OCT is likely to see increasingly widespread use, it is at present important to critically evaluate how this unprecedented view of coronary biology is likely to alter management.

Importantly, outcome data correlating OCT findings with subsequent events is not yet available. This is likely to come from 2 sources. First, clinical trial OCT data are already available on small groups of patients, including those from the ABSORB (a fully absorbable everolimus-eluting stent scaffold: n = 30, follow-up to 3 years) (88), and ODESSA (Optical coherence tomography for DES SAfety) trials (overlapping DES and BMS, n = 71, follow-up: 6 months) (61). These studies demonstrate the precision with which OCT is capable of examining the vascular response to stent placement. Second, close registry follow-up of patients undergoing OCT may provide further important outcome data. One such multicenter registry aims to collate clinical and OCT registry data in 3,000 or more patients, with systematic follow-up for 5 years. This type of clinical trial and registry data will provide opportunities to compare structural changes detected by OCT with clinical outcomes and will be important in establishing whether or not OCT proceeds to a clinically relevant imaging tool.

Some broad comments regarding the clinical use of OCT can be made, however, and are summarized in Table 3. OCT is likely to be useful in the clinical trial evaluation of novel stents and plaque-stabilizing and lipid-lowering drugs, as the information provided by OCT is of particular relevance in these settings and is unique. By contrast, as a result of the requirement for a blood-free field and the poor image penetration, OCT of aorto-ostial lesions, particularly the left main, has not yet proven useful. The use of OCT in saphenous vein graft assessment remains to be established. In the middle ground, in situations where OCT may have a role and be considered, are a large number of potential areas. These include the guiding of complex interventions and stent placement, assessment of NI formation, evaluation of stent thrombosis, and in plaque characterization and possible risk stratification. Although OCT clearly provides detailed images in these situations, a crucial clinical question is whether OCT will replace IVUS for these and similar

contexts. A key factor in this consideration is that data supporting OCT will need to demonstrate improved patient care and improved outcomes. Such indications where this might be foreseen include pre-PCI plaque evaluation; immediate post-PCI evaluation, and assessment of late stent thrombosis. From such considerations, it is clear OCT might either remain a niche-only imaging modality confined to the research arena, or alternatively, evolve into a widely used clinical tool. Investigations in the next few years are likely to be of key importance in determining the ultimate acceptance of intracoronary OCT.

Future Directions and Technical Considerations

OCT is likely to see a number of further developments in the near future, particularly in 2 broad areas. First, widened clinical indications are likely to be explored; some examples include settings of increased NI formation, such as pulmonary hypertension (89), or post-transplantation vasculopathy. Second, a number of technological advances are under active investigation and are expected to yield improved imaging times and image quality for intravascular OCT. Research FD OCT technology has been demonstrated with 100,000 axial scans/s for small animal endoscopic imaging, and acquisition speeds of more than 1 million scans/s have been achieved in bench-top systems using a special swept laser technology (90,91). Future commercial OCT intravascular instruments can be expected to have increases of 2× to 4× the axial scan rates—up to 100,000 to 200,000 axial scans/s. However, intravascular imaging requires mechanical rotation of the catheter imaging optics to generate B-scans, meaning the maximum frame rate (B-scans/s) will likely be limited by the mechanical constraints of catheter rotation. Current intravascular OCT catheters image at 100 frames/s, corresponding to 6,000 rotations per minute. It should be feasible to increase the catheter rotation speeds by ~2× and achieve imaging speeds of approximately 200 frames/s. This increased frame rate will in turn enable a faster pullback speed to image longer segments of the arteries or shorten the procedure time.

Three-dimensional volumetric OCT datasets provide a large amount of data, and improvements in automated image processing can be expected, which will aid in interpretation and analysis (33,47). Parameters, such as sent strut apposition and NI thickness can be readily identified in OCT images and quantitatively measured. However, more subtle morphological parameters, such as fibrous cap thickness, or compositional parameters, such as plaque type, can be more challenging to automate and may still require trained reader interpretation. Automated classification software is especially challenging to develop because of the range of possible morphologies and the requirement that the algorithms achieve sufficient sensitivity and specificity benchmarks to be clinically useful.

A variety of functional OCT imaging techniques are also under investigation. Elastography has been used in IVUS, and analogous techniques are being developed with OCT (92–95). Elastography measures tissue mechanical properties using differences in B-scan images or A-scan acquired at different points in the cardiac cycle. Mechanical properties are an important parameter for the assessment of vulnerable plaque. However, the rapid imaging speeds of intravascular OCT makes this technique challenging because images are acquired rapidly compared with arterial pressure changes. Doppler techniques operate by measuring the changes in the phase of the backscattered light to detect motion. Doppler (96) and polarization-sensitive (97) OCT have been developed and are finding increased use in other specialties, such as ophthalmology. Doppler flow measurements can be integrated with OCT catheter-based structural imaging (98). However, intravascular Doppler OCT is challenging because the optical scattering of blood limits imaging depths, preventing Doppler assessment of the entire cross-sectional luminal flow. In addition, typical OCT imaging catheters would produce perturbations of normal flow. Polarization-sensitive OCT is a promising technique that enhances tissue contrast and specificity by measuring the polarization properties of the backscattered light (99). Last, it is also possible that the use of various macrophage or other cellular targeting agents labeled with fluorophores, such as annexin A5 and other compounds, may allow better characterization of fibrous cap characteristics using hybrid optical systems (100).

Conclusions

OCT is an elegant intravascular imaging modality with unique characteristics, which is already aiding a better understanding of vascular biology. OCT provides detailed structural information, including the vascular responses to PCI, and is establishing itself as a niche device in the evaluation of therapeutic interventions. Importantly, whether this new technology will improve patient care, remains to be seen, and large prospective studies and registry data are already being collected to answer this question.

Reprint requests and correspondence: Dr. Ik-Kyung Jang, Cardiology Division, Massachusetts General Hospital, 55 Fruit Street, GRB 800, Boston, Massachusetts 02114. E-mail: ijang@partners.org.

REFERENCES

1. Huang D, Swanson EA, Lin CP, et al. Optical coherence tomography. Science 1991;254:1178–81.
2. Schuman JS, Puliafito CA, Fujimoto JG, eds. Optical Coherence Tomography of Ocular Diseases. 2nd ed. Thorofare, NJ: Slack, 2004.
3. Chen Y, Aguirre AD, Hsiung PL, et al. Ultrahigh resolution optical coherence tomography of Barrett's esophagus: preliminary descriptive clinical study correlating images with histology. Endoscopy 2007;39:599–605.

4. Raffel OC, Akasaka T, Jang IK. Cardiac optical coherence tomography. Heart 2008;94:1200–10.
5. Mogensen M, Thrane L, Jorgensen TM, et al. OCT imaging of skin cancer and other dermatological diseases. J Biophotonics 2010;2:442–51.
6. Tearney GJ, Waxman S, Shishkov M, et al. Three-dimensional coronary artery microscopy by intracoronary optical frequency domain imaging. J Am Coll Cardiol Img 2008;1:752–61.
7. Brezinski ME, Tearney GJ, Bouma BE, et al. Optical coherence tomography for optical biopsy. Properties and demonstration of vascular pathology. Circulation 1996;93:1206–13.
8. Barlis P, Schmitt JM. Current and future developments in intracoronary optical coherence tomography imaging. EuroIntervention 2009; 4:529–34.
9. Yamaguchi T, Terashima M, Akasaka T, et al. Safety and feasibility of an intravascular optical coherence tomography image wire system in the clinical setting. Am J Cardiol 2008;101:562–7.
10. Kubo T, Imanishi T, Takarda S, et al. Assessment of culprit lesion morphology in acute myocardial infarction: ability of optical coherence tomography compared with intravascular ultrasound and coronary angioscopy. J Am Coll Cardiol 2007;50:933–9.
11. Jang IK. Optical coherence tomography or intravascular ultrasound? J Am Coll Cardiol Intv 2011;4:492–4.
12. Bezerra HG, Costa MA, Guagliumi G, et al. Intracoronary optical coherence tomography: a comprehensive review. J Am Coll Cardiol Intv 2009;2:1035–46.
13. Yabushita H, Bouma BE, Houser SL, et al. Characterization of human atherosclerosis by optical coherence tomography. Circulation 2002;106:1640–5.
14. Kume T, Akasaka T, Kawamoto T, et al. Assessment of coronary arterial plaque by optical coherence tomography. Am J Cardiol 2006;97:1172–5.
15. Kawasaki M, Bouma BE, Bressner J, et al. Diagnostic accuracy of optical coherence tomography and integrated backscatter intravascular ultrasound images for tissue characterization of human coronary plaques. J Am Coll Cardiol 2006;48:81–8.
16. Manfrini O, Mont E, Leone O, et al. Sources of error and interpretation of plaque morphology by optical coherence tomography. Am J Cardiol 2006;98:156–9.
17. Rieber J, Meissner O, Babaryka G, et al. Diagnostic accuracy of optical coherence tomography and intravascular ultrasound for the detection and characterization of atherosclerotic plaque composition in ex-vivo coronary specimens: a comparison with histology. Coron Artery Dis 2006;17:425–30.
18. Tearney GJ, Yabushita H, Houser SL, et al. Quantification of macrophage content in atherosclerotic plaques by optical coherence tomography. Circulation 2003;107:113–9.
19. Brezinski ME. Optical coherence tomography for identifying unstable coronary plaque. Int J Cardiol 2006;107:154–65.
20. Burke AP, Farb A, Malcom GT, Liang YH, Smialek J, Virmani R. Coronary risk factors and plaque morphology in men with coronary disease who died suddenly. N Engl J Med 1997;336:1276–82.
21. Kume T, Akasaka T, Kawamoto T, et al. Measurement of the thickness of the fibrous cap by optical coherence tomography. Am Heart J 2006;152:755e1–4.
22. Jang I-K, Bouma BE, Kang DH, et al. Visualization of coronary atherosclerotic plaques in patients using optical coherence tomography: comparison with intravascular ultrasound. J Am Coll Cardiol 2002;39:604–9.
23. Kume T, Akasaka T, Kawamoto T, et al. Assessment of coronary arterial thrombus by optical coherence tomography. Am J Cardiol 2006;97:1713–7.
24. Meng L, Lv B, Zhang S, Yv B. In vivo optical coherence tomography of experimental thrombosis in a rabbit carotid model. Heart 2008;94: 777–80.
25. Tearney GJ, Jang I-K, Kang DH, et al. Porcine coronary imaging in vivo by optical coherence tomography. Acta Cardiol 2000;55:233–7.
26. Prati F, Regar E, Mintz GS, et al. Expert review document on methodology, terminology, and clinical applications of optical coherence tomography: physical principles, methodology of image acquisition, and clinical application for assessment of coronary arteries and atherosclerosis. Eur Heart J 2010;31:401–15.
27. Jang I-K, Tearney GJ, MacNeill BD, et al. In vivo characterization of coronary atherosclerotic plaque by use of optical coherence tomography. Circulation 2005;111:1551–5.
28. Takarada S, Imanishi T, Kubo T, et al. Effect of statin therapy on coronary fibrous-cap thickness in patients with acute coronary syndrome: assessment by optical coherence tomography study. Atherosclerosis 2009;202:491–7.
29. Chia S, Raffel OC, Takano M, Tearney GJ, Bouma BE, Jang IK. Association of statin therapy with reduced coronary plaque rupture: an optical coherence tomography study. Coron Artery Dis 2008;19:237–42.
30. Tanaka A, Imanishi T, Kitabata H, et al. Morphology of exertion-triggered plaque rupture in patients with acute coronary syndrome: an optical coherence tomography study. Circulation 2008;118:2368–73.
31. Yonetsu T, Kakuta T, Lee T, et al. Impact of plaque morphology on creatine kinase-MB elevation in patients with elective stent implantation. Int J Cardiol 2011;146:80–5.
32. MacNeill BD, Jang IK, Bouma BE, et al. Focal and multi-focal plaque macrophage distributions in patients with acute and stable presentations of coronary artery disease. J Am Coll Cardiol 2004;44: 972–9.
33. van Soest G, Goderie T, Regar E, et al. Atherosclerotic tissue characterization in vivo by optical coherence tomography attenuation imaging. J Biomed Opt 2010;15:011105.
34. Tanaka A, Tearney GJ, Bouma BE. Challenges on the frontier of intracoronary imaging: atherosclerotic plaque macrophage measurement by optical coherence tomography. J Biomed Opt 2010;15: 011104.
35. Vorpahl M, Nakano M, Virmani R. Small black holes in optical frequency domain imaging matches intravascular neoangiogenesis formation in histology. Eur Heart J 2010;31:1889.
36. Brown EN, Burris NS, Gu J, et al. Thinking inside the graft: applications of optical coherence tomography in coronary artery bypass grafting. J Biomed Opt 2007;12:051704.
37. Tyczynski P, Kukreja N, van Geuns RJ, Wykrzykowska JJ, Sheppard MN, Di Mario C. Optical coherence tomography for the assessment of pericardium covered stents for the treatment of degenerated saphenous vein grafts. EuroIntervention 2010;6:78–85.
38. Yonetsu T, Kakuta L, Lee T, et al. Assessment of acute injuries and chronic intimal thickening of the radial artery after transradial coronary intervention by optical coherence tomography. Eur Heart J 2010;31:1605–15.
39. Diaz-Sandoval LJ, Bouma BE, Tearney GJ, Jang IK. Optical coherence tomography as a tool for percutaneous coronary interventions. Catheter Cardiovasc Interv 2005;65:492–6.
40. Jang I-K, Tearney GJ, Bouma BE. Visualization of tissue prolapse between coronary stent struts by optical coherence tomography: comparison with intravascular ultrasound. Circulation 2001;104:2754.
41. Bouma BE, Tearney GJ, Yabushita H, et al. Evaluation of intracoronary stenting by intravascular optical coherence tomography. Heart 2003;89:317–20.
42. Gonzalo N, Serruys PW, Okamura T, et al. Optical coherence tomography assessment of the acute effects of stent implantation on the native vessel wall: a systematic quantitative approach. Heart 2010;95:1913–9.
43. Farb A, Sangiorgi G, Carter AJ, et al. Pathology of acute and chronic coronary stenting in humans. Circulation 1999;99:44–52.
44. Kim SW, Mintz GS, Ohlmann P, et al. Frequency and severity of plaque prolapse within Cypher and Taxus stents as determined by sequential intravascular ultrasound analysis. Am J Cardiol 2006;98:1206–11.
45. Gonzalo N, Serruys PW, Okamura T, et al. Relation between plaque type and dissections at the edges after stent implantation: an optical coherence tomography study. Int J Cardiol 2011;150:151–5.
46. Tanigawa J, Barlis P, Dimopoulos K, Dalby M, Moore P, Di Mario C. The influence of strut thickness and cell design on immediate apposition of drug-eluting stents assessed by optical coherence tomography. Int J Cardiol 2009;134:180–8.
47. Barlis P, Dimopoulos K, Tanigawa J, et al. Quantitative analysis of intracoronary optical coherence tomography measurements of stent strut apposition and tissue coverage. Int J Cardiol 2010;141:151–6.

48. Takano M, Inami S, Jang I-K, et al. Evaluation by optical coherence tomography of neointimal coverage of sirolimus-eluting stent three months after implantation. Am J Cardiol 2007;99:1033–8.
49. Zreiqat H, James B, Brieger D, Kritharides L, Lowe HC. Acute coronary stent thrombosis: toward insights into possible mechanism using novel imaging methods. Thromb Haemost 2008;99:976–7.
50. Nakazawa G, Finn AV, Joner M, et al. Delayed arterial healing and increased late stent thrombosis at culprit sites after drug-eluting stent placement for acute myocardial infarction patients: an autopsy study. Circulation 2008;118:1138–45.
51. Tanimoto S, Rodrigues-Granillo G, Barlis P, et al. A novel approach for quantitative analysis of intracoronary optical coherence tompgraphy: high inter-observer agreement with computer-assisted contour detection. Catheter Cardiovasc Interv 2008;72:228–35.
52. Sihan K, Botha C, de Winter S, et al. Fully automatic three-dimensional quantitative analysis of intracoronary optical coherence tomography: method and validation. Catheter Cardiovasc Interv 2008;74:1058–65.
53. Andreopoulos B, An A, Wang X, Schroeder M. A roadmap of clustering algorithms: finding a match for a biomedical application. Brief Bioinform 2009;10:297–314.
54. Guagliumi G, Musumeci G, Sirbu V, et al. Optical coherence tomography assessment of in vivo vascular response after implantation of overlapping bare-metal and drug-eluting stents. J Am Coll Cardiol Intv 2010;3:531–9.
55. Chen BX, Ma FY, Luo W, et al. Neointimal coverage of bare-metal and sirolimus-eluting stents evaluated with optical coherence tomography. Heart 2007;94:566–70.
56. Xie Y, Takano M, Murakami D, et al. Comparison of neointimal coverage by optical coherence tomography of a sirolimus-eluting stent versus a bare-metal stent three months after implantation. Am J Cardiol 2008;102:27–31.
57. Yao Z-H, Matsubara T, Inada T, Suzuki Y, Suzuki T. Neointimal coverage of sirolimus-eluting stents 6 months and 12 months after implantation: evaluation by optical coherence tomography. Chin Med J (Engl) 2008;121:503–7.
58. Kim J-S. Kim J-S, Kim TH, et al. Comparison of neointimal coverage of sirolimus-eluting stents and paclitaxel-eluting stents using optical coherence tomography at 9 months after implantation. Circ J 2010; 74:320–6.
59. Kim J-S. Jang I-K, Kim J-S, et al. Optical coherence tomography evaluation of zotarolimus-eluting stents at 9 month follow-up: comparison with sirolimus-eluting stents. Heart 2009;95:1907–12.
60. Katoh H, Shite J, Shinke T, et al. Delayed neointimalization on sirolimus-eluting stents: 6 month and 12 month follow-up by optical coherence tomography. Circ J 2009;73:1033–7.
61. Tahara S, Bezerra HG, Sirbu V, et al. Angiographic, IVUS and OCT evaluation of the long-term impact of coronary disease severity at the site of overlapping drug-eluting and bare metal stents: a substudy of the ODESSA trial. Heart 2010;96:1574–8.
62. Guagliumi G, Sirbu V, Bezerra HG, et al. Strut coverage and vessel wall response to zotarolimus-eluting and bare-metal stents implanted in patients with ST-segment elevation myocardial infarction: the OCTAMI (Optical Coherence Tomography in Acute Myocardial Infarction) study. J Am Coll Cardiol Intv 2010;3:680–7.
63. Murata A, Wallace-Bradley D, Tellez A, et al. Accuracy of optical coherence tomography in the evaluation of neointimal coverage after stent implantation. J Am Coll Cardiol Img 2010;3:76–84.
64. Barlis P, Regar E, Serruys PW, et al. An optical coherence tomography study of a biodegradable vs. durable polymer-coated limus-eluting stent: a LEADERS trial sub-study. Eur Heart J 2010;31:165–76.
65. Gonzalo N, Serruys PW, García-García HM, et al. Quantitative ex vivo and in vivo comparison of lumen dimensions measured by optical coherence tomography and intravascular ultrasound in human coronary arteries. Rev Esp Cardiol 2009;62:615–24.
66. Templin C, Meyer M, Müller FM, et al. Coronary optical frequency domain imaging (OFDI) for in vivo evaluation of stent healing: comparison with light and electron microscopy. Eur Heart J 2010;31: 1792–801.
67. Inoue T, Shite J, Yoon J, et al. Optical coherence evaluation for everolimus-eluting stents at 8 months after implantation (Cooperative Study with Korea). Heart 2011;97:1379–84.
68. Mintz GS, Weissman NJ, Fitzgerald PJ. Intravascular ultrasound assessment of the mechanisms and results of brachytherapy. Circulation 2001;104:1320–5.
69. Shah VM, Mintz GS, Apple S, Weissman NJ. Background incidence of late malapposition after bare-metal stent implantation. Circulation 2002;106:1753–5.
70. Matsumoto D, Shite J, Shinke T, et al. Neointimal coverage of sirolimus-eluting stents at 6-month follow-up: evaluated by optical coherence tomography. Eur Heart J 2007;28:961–7.
71. Ishigami K, Uemura S, Morikawa Y, et al. Long term follow-up of neointimal coverage of sirolimus-eluting stents. Circ J 2009;73: 2300–7.
72. Kim J-S, Hong M-K, Fan C, et al. Intracoronary thrombus formation after drug-eluting stents implantation: optical coherence tomographic study. Am Heart J 2010;159:278–83.
73. Miyoshi N, Shite J, Shinke T, et al. Comparison by optical coherence tomography of paclitaxel-eluting stents with sirolimus-eluting stents implanted in one coronary artery in one procedure. Circ J 2010;74:903–8.
74. Webster MW, Ormiston JA. Sorting out drug-eluting stents. Lancet 2010;375:1060–1.
75. Murakami D, Takano M, Yamamoto M, et al. Advanced neointimal growth is not associated with a low risk of in-stent thrombus. Circ J 2009;73:1627–34.
76. Gonzalo N, Serruys PW, Okamura T, et al. Optical coherence tomography patterns of stent restenosis. Am Heart J 2009;158:284–93.
77. Suzuki N, Kozuma K, Maeno Y, et al. Quantitative coronary optical coherence tomography image analysis for the signal attenuation observed in-stent restenotic tissue. Int J Cardiol 2010;145:392–4.
78. Yamamoto M, Takano M, Murakami D, et al. Optical coherence tomography analysis for restenosis of drug-eluting stents. Int J Cardiol 2011;146:100–3.
79. Barlis P, van Soest G, Serruys PW, Regar E. Intracoronary optical coherence tomography and the evaluation of stents. Expert Rev Med Dev 2009;6:157–67.
80. Farb A, Burke AP, Kolodgie FD, Virmani R. Pathological mechanisms of fatal late coronary stent thrombosis in humans. Circulation 2003;108:1701–6.
81. Nagai H, Ishibashi-Ueda H, Fujii K. Histology of highly echolucent regions in optical coherence tomography images from two patients with sirolimus-eluting stent restenosis. Catheter Cardiovasc Interv 2010;75:961–3.
82. Teramoto T, Ikeno F, Otake H, et al. Intriguing peri-strut low intensity area detected by optical coherence tomography after coronary stent deployment. Circ J 2010;74:1257–9.
83. Takano M, Yamamoto M, Inami S, et al. Appearance of lipid-laden intima and neovascularization after implantation of bare metal stents. J Am Coll Cardiol 2010;55:26–32.
84. Hou J, Qi H, Zhang M, et al. Development of lipid-rich plaque inside bare metal stent: possible mechanism of late stent thrombosis? An optical coherence tomography study. Heart 2010;96:1187–90.
85. Higo T, Ueda Y, Oyabu J, et al. Atherosclerotic and thombogenic neointima formed over sirolimus drug-eluting stent: an angioscopic study. J Am Coll Cardiol Img 2009;2:616–24.
86. Nakazawa G, Vorpahl M, Finn AV, et al. One step forward and two steps back with drug-eluting stents. J Am Coll Cardiol Img 2009;2:625–8.
87. Moharram MA, Yeoh T, Lowe HC. Swings and roundabouts: intravascular optical coherence tomography (OCT) in the evaluation of the left main stem coronary artery. Int J Cardiol 2011;148:243–4.
88. Onuma Y, Serruys PW, Ormiston JA, et al. Three-year results of clinical follow-up after a bioresorbable everolimus-eluting scaffold in patients with de novo coronary artery disease: the ABSORB trial. EuroIntervention 2010;6:447–53.
89. Hou J, Qi H, Zhang M, et al. Pulmonary vascular changes in pulmonary hypertension: optical coherence tomography findings. Circ Cardiovasc Imaging 2010;3:344–5.
90. Adler DC, Chen Y, Huber R, et al. Three dimensional endomicroscopy using optical coherence tomography. Nat Photonics 2007;1: 709–16.

91. Wieser W, Biedermann BR, Klein T, Eigenwillig CM, Huber R. Multi-megahertz OCT: high quality 3D imaging at 20 million A-scans and 4.5 Gvoxels per second. Opt Express 2010;18:14685–704.
92. Schmitt JM. OCT elastography: imaging microscopic deformation and strain of tissue. Opt Express 1998;3:199–211.
93. Chan R, Chau A, Karl W, et al. OCT-based arterial elastography: robust estimation exploiting tissue biomechanics. Opt Express 2004; 12:4558–72.
94. Rogowska J, Patel N, Plummer S, Brezinski ME. Quantitative optical coherence tomographic elastography: method for assessing arterial mechanical properties. Br J Radiol 2006;79:707–11.
95. van Soest G, Mastik F, de Jong N, van der Steen AF. Robust intravascular optical coherence elastography by line correlations. Phys Med Biol 2007;52:2445–8.
96. Leitgeb RA, Schmetterer L, Drexler W, Fercher A, Zawadzki R, Bajraszewski T. Real-time assessment of retinal blood flow with ultrafast acquisition by color Doppler Fourier domain optical coherence tomography. Opt Express 2003;11:3116–21.
97. Cense B, Mujat M, Chen TC, Park BH, de Boer JF. Polarization-sensitive spectral-domain optical coherence tomography using a single line scan camera. Opt Express 2007;15:2421–31.
98. Li H, Standish BA, Mariampillai A, et al. Feasibility of interstitial Doppler optical coherence tomography for in vivo detection of microvascular changes during photodynamic therapy. Lasers Surg Med 2006;38:754–61.
99. Giattina SD, Courtney BK, Herz PR, et al. Assessment of coronary plaque collagen with polarization sensitive optical coherence tomography (PS-OCT). Int J Cardiol 2006;107:400–9.
100. Tahara N, Imaisumi T, Virmani R, Narula J. Clinical feasibility of molecular imaging of plaque inflammation in atherosclerosis. J Nucl Med 2009;50:331–4.

Key Words: atherosclerosis ■ coronary stent ■ intravascular imaging.